Redox Biology 70 (2024) 103035

Contents lists available at ScienceDirect

Redox Biology

journal homepage: www.elsevier.com/locate/redox

DNAJC12 causes breast cancer chemotherapy resistance by repressing doxorubicin-induced ferroptosis and apoptosis via activation of AKT

Mengjia Shen [a,b], Shiyu Cao [b], Xinyi Long [b], Lin Xiao [b], Libo Yang [a,b], Peichuan Zhang [d], Li Li [b], Fei Chen [b], Ting Lei [e], Hongwei Gao [f], Feng Ye [b,c,**], Hong Bu [a,b,c,*]

[a] Department of Pathology, West China Hospital, Sichuan University, No. 37, Guo Xue Xiang, Chengdu, 610041, Sichuan, China
[b] Institute of Clinical Pathology, West China Hospital, Sichuan University, Chengdu, 610041, Sichuan, China
[c] Key Lab of Transplant Engineering and Immunology, Ministry of Health, West China Hospital, Sichuan University, Chengdu, 610041, Sichuan, China
[d] Institute of Thoracic Oncology and Department of Thoracic Surgery, West China Hospital, Sichuan University, Chengdu, China
[e] Department of Pathology, The Third Affiliated Hospital of Soochow University, Changzhou, Jiangsu 213003, China
[f] Laboratory Medicine Center, Lanzhou University Second Hospital, The Second Clinical Medical College of Lanzhou University, Lanzhou 730000, China

ARTICLE INFO

Keywords:
DNAJC12
Breast cancer
HSP70
AKT
Ferroptosis
Apoptosis

ABSTRACT

Background: Chemotherapy is a primary treatment for breast cancer (BC), yet many patients develop resistance over time. This study aims to identify critical factors contributing to chemoresistance and their underlying molecular mechanisms, with a focus on reversing this resistance.

Methods: We utilized samples from the Gene Expression Omnibus (GEO) and West China Hospital to identify and validate genes associated with chemoresistance. Functional studies were conducted using MDA-MB-231 and MCF-7 cell lines, involving gain-of-function and loss-of-function approaches. RNA sequencing (RNA-seq) identified potential mechanisms. We examined interactions between DNAJC12, HSP70, and AKT using co-immunoprecipitation (Co-IP) assays and established cell line-derived xenograft (CDX) models for *in vivo* validations.

Results: Boruta analysis of four GEO datasets identified DNAJC12 as highly significant. Patients with high DNAJC12 expression showed an 8 % pathological complete response (pCR) rate, compared to 38 % in the low expression group. DNAJC12 inhibited doxorubicin (DOX)-induced cell death through both ferroptosis and apoptosis. Combining apoptosis and ferroptosis inhibitors completely reversed DOX resistance caused by DNAJC12 overexpression. RNA-seq suggested that DNAJC12 overexpression activated the PI3K-AKT pathway. Inhibition of AKT reversed the DOX resistance induced by DNAJC12, including reduced apoptosis and ferroptosis, restoration of cleaved caspase 3, and decreased GPX4 and SLC7A11 levels. Additionally, DNAJC12 was found to increase AKT phosphorylation in an HSP70-dependent manner, and inhibiting HSP70 also reversed the DOX resistance. In vivo studies confirmed that AKT inhibition reversed DNAJC12-induced DOX resistance in the CDX model.

Conclusion: DNAJC12 expression is closely linked to chemoresistance in BC. The DNAJC12-HSP70-AKT signaling axis is crucial in mediating resistance to chemotherapy by suppressing DOX-induced ferroptosis and apoptosis. Our findings suggest that targeting AKT and HSP70 activities may offer new therapeutic strategies to overcome chemoresistance in BC.

1. Introduction

Breast cancer (BC) stands as one of the prevalent malignancies globally [1]. In China, it holds the top position in incidence and the second position in mortality among cancers affecting the female population [1]. Neoadjuvant chemotherapy has emerged as a widely recommended approach for treating breast cancer due to its benefits in reducing tumor size before surgery and assessing drug effectiveness *in vivo* [2]. Despite the favorable prognosis associated with estrogen receptor (ER) positivity, this subgroup exhibits significant insensitivity to

* Corresponding author.Institute of Clinical Pathology, West China Hospital, Sichuan University, Chengdu, 610041, Sichuan, China
** Corresponding author. Institute of Clinical Pathology, West China Hospital, Sichuan University, Chengdu, 610041, Sichuan, China
E-mail addresses: fengye@scu.edu.cn (F. Ye), hongbu@scu.edu.cn (H. Bu).

https://doi.org/10.1016/j.redox.2024.103035
Received 10 December 2023; Received in revised form 3 January 2024; Accepted 7 January 2024
Available online 24 January 2024

chemotherapy. Overcoming chemotherapy resistance in this category could enhance the survival rate for ER-positive individuals. While triple-negative breast cancer demonstrates heightened sensitivity to chemotherapy compared to other subtypes, a considerable number of patients develop drug resistance after a period of treatment. This phenomenon limits available regimens for subsequent treatment and results in unfavorable clinical outcomes [3]. Thus, the identification of key factors contributing to the chemoresistance of breast cancer, coupled with efforts to reverse this process, holds promise for improving the treatment efficacy and ultimately enhancing the 5-year overall survival rate for patients.

Upon reanalyzing the mRNA expression profiles of 933 patients subjected to neoadjuvant chemotherapy, our investigation identified DnaJ heat shock protein family (Hsp40) member C12 (DNAJC12) as the foremost factor in Boruta analysis for gauging neoadjuvant chemotherapy response. Positioned on chromosome 10q21.3 (10q21.1), DNAJC12 encodes a protein affiliated with the Hsp40/DnaJ family, characterized by a J domain [4]. Members of this subclass are known to frequently engage as cochaperone proteins, directly interacting with Hsp70 and Hsp 90 [5,6]. DNAJC12 specifically interacts with the DNA binding domain (DBD) of the progesterone receptor (PR), without stimulating PR activity or affecting its transactivation properties [7]. The mRNA expression of DNAJC12 correlates directly with the estrogen receptor (ER) status in breast tumors, suggesting potential transcriptional regulation by estrogen. Additionally, DNAJC12 can elevate ERBB4 expression [8,9]. Notably, administration of tamoxifen leads to a significant downregulation of DNAJC12 [10]. Furthermore, DNAJC12 plays a role in the onset, progression, and prognosis of various tumors [11–14]. Importantly, DNAJC12 overexpression emerges as a negative predictor for neoadjuvant concurrent chemoradiotherapy (CCRT) response [15].

Anthracycline-based regimens are standard in neoadjuvant chemotherapy, with apoptosis being a key pathway. However, focusing solely on apoptosis overlooks other potential death pathways, which emerge under drug resistance pressures. Our study is the first to report doxorubicin (DOX)-induced ferroptosis in a DNAJC12-dependent manner. Ferroptosis is a recently identified cell death pathway involving lipid peroxidation, influenced by factors such as iron levels, cysteine metabolism, GPX4 activity, and System Xc-, among others [16,17]. System Xc-facilitates the exchange of glutamate and cystine across the plasma membrane, with cysteine acting as the rate-limiting amino acid for glutathione (GSH) synthesis [18,19]. GSH serves as the GPX4 cofactor, protecting cells from lipid peroxides. The GPX4 pathway mitigates toxic phospholipid hydroperoxides by oxidizing GSH into oxidized glutathione (GSSG), thus inhibiting ferroptosis [17,20,21]. The growing body of research has unveiled the connection between ferroptosis and cancer, positioning the induction of ferroptosis as a novel strategy to combat cancer [22,23]. Doxorubicin treatment induces alterations in iron metabolism through diverse mechanisms [24]. A study demonstrated that DOX-induced heme oxygenase-1 (HO-1) upregulation leads to nonheme iron accumulation via heme degradation, subsequently triggering lipid peroxidation and ferroptosis. In this context, ferroptosis inhibitors prove effective in preventing DOX-induced cardiomyopathy [25]. Notably, existing research on DOX and ferroptosis has primarily concentrated on the adverse effects on cardiomyocytes [26], with no investigations into the induction of ferroptosis by DOX, let alone its impact on DOX resistance in tumor cells.

This study unveiled how DNAJC12 contributes to BC chemoresistance by inhibiting ferroptosis and apoptosis. We demonstrated the pivotal role of the DNAJC12-HSP70-AKT signaling axis in this resistance and showed that AKT or HSP70 inhibitors could reverse this process. These findings offer novel therapeutic approaches to combat BC chemoresistance.

2. Materials and methods

2.1. Gene expression microarray data collection

Selected from the Gene Expression Omnibus (GEO), datasets exclusively encompassed breast cancer patients undergoing taxane or anthracycline-based neoadjuvant chemotherapy. Exclusions comprised datasets involving HER2-positive patients receiving targeted therapy. The final analysis focused on four datasets (GSE41998, GSE25065, GSE20194, GSE20271) meeting the specified criteria. Retrieval of mRNA expression profiles and clinicopathologic features utilized GEO database accession numbers associated with these datasets.

2.2. Clinical sampling

A total of 115 breast cancer samples were obtained from West China Hospital of Sichuan University (IRS number: 2017–476). All patients underwent neoadjuvant chemotherapy with anthracycline or taxane, excluding targeted therapy. Pathologic complete response (pCR) denoted ypT0/is, indicating the absence of residual invasive disease. ER, PR, and HER2 status in pre-neoadjuvant chemotherapy formalin-fixed paraffin-embedded (FFPE) tissues were assessed via immunohistochemistry (IHC). Positive ER and PR statuses required positively stained nuclei in $\geq$1 % of tumor tissues. HER2 positivity was defined as IHC 3+ or fluorescence *in situ* hybridization (FISH)-amplified HER2.

2.3. Quantitative reverse transcription PCR (RT–qPCR)

Total RNA extraction utilized the RNA-Quick Purification Kit (ES Science, China) for cells and the RNeasy FFPE Kit (QIAGEN, Germany) for FFPE samples. RNA concentration was measured using Nanodrop One (Thermo Scientific, USA). Reverse transcription of 1 μg RNA from both FFPE samples and cells into cDNA was achieved separately using the Omniscript RT Kit (QIAGEN, Germany) and 5 × EasyQuick RT Master Mix (CWBIO, China) on a T100 thermal cycler (Bio-Rad, USA). RT–qPCR employed TaKaRa Taq Hot Start Version (TaKaRa, Japan) for FFPE samples and AceQ qPCR SYBR Green Master Mix (Vazyme, China) for cells on a 7300 Plus Real-Time PCR System. The relative expression of targeted genes was calculated using formula 2^(−ΔCt) with reference genes. Supplementary Table 1 presents the primer details.

2.4. Chemicals

The ferroptosis inducer RSL3 (HY-100218 A), HSP70 inhibitor apoptozole (HY-15098), VER-155008 (HY-10941), and AKT inhibitor capivasertib (HY-15431) were procured from MedChemExpress. Additionally, Doxorubicin HCl (CSN16255), docetaxel (CSN12495), the apoptosis inhibitor *Z*-VAD-FMK (CSN19230), and the ferroptosis inhibitor ferrostatin-1 (CSN12654) were sourced from CSNpharm.

2.5. Cell culture and transfection

MDA-MB-231 and MCF-7 cells, acquired from the Stem Cell Bank, Chinese Academy of Sciences and authenticated by Genetic Testing Biotechnology Corporation (Suzhou, China), were cultured in RPMI 1640 medium (Gibco, USA) supplemented with 10 % fetal bovine serum (FBS) (Gibco, USA) and 1 % penicillin/streptomycin at 37 °C with 5 % CO_2. The shDNAJC12 and Flag-tagged DNAJC12v plasmids were obtained from GeneChem (Shanghai, China), and DNAJC12 siRNA was sourced from GenePharma (Shanghai, China). Transfection of cells with plasmid DNA or siRNA employed Lipofectamine 3000 (Life Technologies, USA) following the manufacturer's instructions. Supplementary Tables 2–3 provide the sequences of siRNAs and plasmids.

2.6. Cell viability and colony formation assay

Cell viability and drug sensitivity were assessed through cell proliferation assays. In 96-well culture plates (Thermo, USA), $6 \times 10^{\hat{}}3$ cells/well were seeded 24 h prior to drug treatment. Following a 48-h exposure to varying chemical concentrations, cell viability was determined using the CCK-8 assay with the EnoGeneCell™ Counting Kit-8 (Enogene, China), following the manufacturer's instructions. For the colony formation assay, 1000 cells/well were seeded in 6-well plates, incubated for 14 days, and subsequently washed and stained with a 0.05 % crystal violet solution. The quantification involved counting the colonies containing more than 10 cells.

2.7. Cell apoptosis detection

Apoptosis in cells was assessed using an Annexin V-Alexa Fluor 647/PI Kit (4 A Biotech, China) following the manufacturer's instructions. DAPI replaced PI during DOX treatment due to fluorescence interference. Flow cytometry on a CytoFLEX Flow Cytometer (Beckman Coulter, USA) captured 20,000 cells for targeted events. FlowJo_V10 software facilitated the analysis of the apoptotic population.

2.8. C11-BODIPY staining

Cells were cultured in 6-well plates (Thermo, USA) until reaching confluence. Following pretreatment with DOX or ferroptosis inducer RSL3 for 24 h, cells were washed and incubated with 2 μmol/L C11-BODIPY (Invitrogen, USA) for 30 min, followed by fixation with 4 % paraformaldehyde for fluorescence imaging. Additionally, after DOX or RSL3 pretreatment, cells were collected, stained with 2 μmol/L C11-BODIPY for 30 min, and subjected to flow cytometry for fluorescence intensity estimation.

2.9. Malondialdehyde (MDA) assay

Cells were seeded in 6-well plates, and treatments were in accordance with the C11-BODIPY assay. Following treatment, cells were harvested for protein extraction. Protein concentrations were determined using a BCA protein assay kit (Thermo, USA), while MDA concentrations were quantified with a lipid peroxidation MDA assay kit (Beyotime, China) as per the provided instructions. The MDA-to-protein concentration ratio was then calculated. It is important to note potential artifacts in the measurement of lipid peroxidation due to the reaction of thiobarbituric acid (TBA) with MDA. TBA may readily react with other cellular substrates, such as alkanals, proteins, and urea, leading to a significant increase in the assay's product levels [27].

2.10. Determination of intracellular labile iron

Labile iron content in MDA-MB-231 and MCF-7 cells was assessed using the Fe^{2+} fluorescent probe FerroOrange (MKBio, China). Cells were cultured in 6-well plates and pre-treated with doxorubicin for 48 h. Subsequently, cells were washed and incubated with 1 μmol/L FerroOrange for 30 min, and fluorescence intensity were acquired.

2.11. RNA-seq analysis

Total RNA from $5 \times 10^{\hat{}}6$ cells was extracted using TRIzol (Cwbiotech, China). After qualification via an Agilent 2100 bioanalyzer, the qualified RNA was employed to construct an RNA library. Transcriptome sequencing utilized the Illumina NovaSeq platform. HISAT2 software mapped reads to the human genome (UCSC hg38). Gene expression levels were estimated with the featureCounts tool of subread software and stringtie. Differential expression analysis employed the edgeR and DESeq2 R packages, considering $P < 0.05$ or $|\log 2$ (fold change)$| > 1$ as significant. KEGG and GO enrichment analyses were performed using the clusterProfiler R package. GSEA utilized the local version (http://www.broadinstitute.org/gsea/index.jsp) across different datasets.

2.12. Western blot

Total protein extraction and quantification utilized radioimmunoprecipitation assay (RIPA) buffer (Sigma Aldrich, USA) and a BCA Protein Assay Kit (Thermo, USA) respectively. SDS–PAGE (Thermo, USA) separated 20 μg of protein lysates, subsequently transferred to polyvinylidene fluoride membranes (Millipore, Germany). Specific antibodies against GAPDH (1:2000, ZENBIO, China), DNAJC12 (1:2000, Abcam, UK), β-Actin (1:2000, Cloud-Clone Corp, China), HSP70 (1:2000, Abcam, UK), SLC7A11 (1:2000, Abcam, UK), GPX4 (1:2000, Abcam, UK), caspase 3 (1:2000, Proteintech, US), *p*-AKT1 (1:2000, Abcam, UK), AKT1 (1:2000, Proteintech, US), and DDDDK tag (1:2000, Abcam, UK) were employed to incubate with the cut bands.

2.13. CDX model in vivo study

Immunodeficient BALB/c nude female mice (4 weeks old) obtained from GemPharmtech (Jiangsu, China) were utilized. MDA-MB-231 cells ($2 \times 10^{\hat{}}6$) in the DNAJC12 overexpression (OE) and negative control (NC) groups were subcutaneously injected. Once tumors reached 100 mmˆ3, mice were randomly divided into eight groups (4 mice per group) and intraperitoneally administered capivasertib (50 mg/kg), doxorubicin HCl (5 mg/kg), or a combination of capivasertib and doxorubicin HCl every three days for a total of 5 injections. Doxorubicin HCl dosage was determined based on preliminary experiments, with doses of 12, 10, 5, and 2 mg/kg tested. A dose of 5 mg/kg was selected considering tumor inhibition rate and the health status of nude mice. Tumor dimensions were measured using a digital caliper, and formula $V = 1/2$ (length $\times$ width$^{\hat{}}2$) calculated tumor volume. IACUC approval (No. 20211507 A) was obtained for this study.

2.14. Immunohistochemistry (IHC)

Immunohistochemistry evaluated protein expression of DNAJC12, *p*-AKT, GPX4, and SLC7A11 in mouse tumor samples from the DNAJC12 overexpression (OE) and negative control (NC) groups. Antibodies and dilutions were as follows: DNAJC12 (1:200, ab254762, Abcam), *p*-AKT1 (pS473) (1:200, 2118–1, EPITOMICS), GPX4 (1:200, ab125066, Abcam), and SLC7A11 (1:200, ab175186, Abcam).

2.15. Statistical analysis

Boruta analysis, employed on the four selected GEO datasets, facilitated feature selection to identify predictors of neoadjuvant chemotherapy response. Mean ± standard deviation (SD) presented the data. SPSS 25.0 statistical software conducted the statistical analysis, and GraphPad Prism 7 generated graphics. Chi-squared tests determined the relationship between clinicopathological characteristics and neoadjuvant chemotherapy response. Group comparisons utilized unpaired, 2-tailed t-tests or one-way ANOVA. Pearson's correlation coefficient analyzed correlations, while univariate and multivariate regression analyses explored potential predictors. A significance level of $P < 0.05$ was applied.

3. Results

3.1. High DNAJC12 expression is associated with chemotherapy resistance in BC

To identify the pivotal determinant influencing the effect of neoadjuvant chemotherapy based on anthracycline and taxanes, an analysis of four Gene Expression Omnibus (GEO) datasets was undertaken.

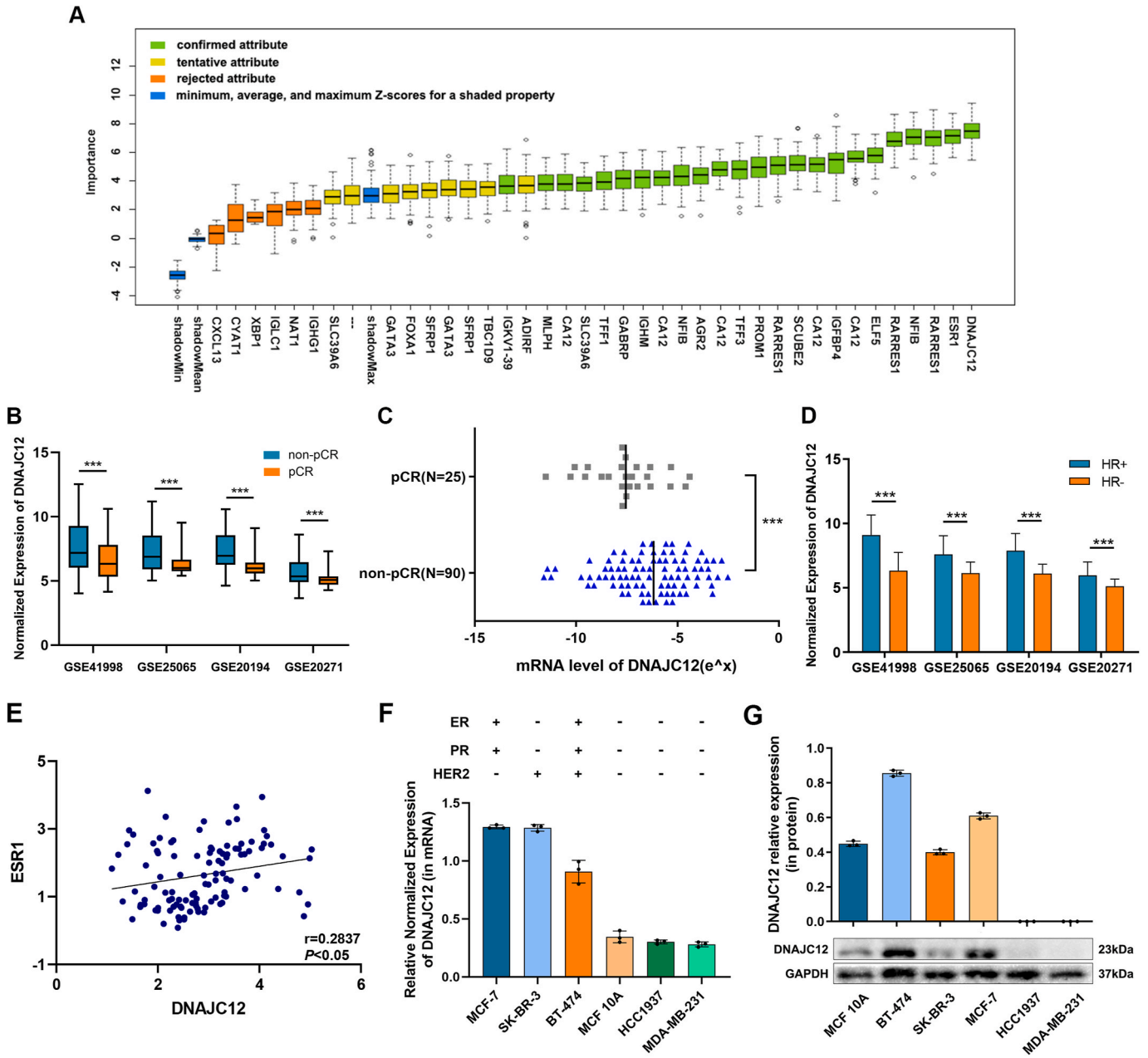

Fig. 1. DNAJC12 is overexpressed in non-pCR and HR+ breast cancer. A. Boruta analysis of neoadjuvant chemotherapy-related characteristics in four GEO datasets. **B.** DNAJC12 expression in non-pCR and pCR patients in four GEO datasets. **C.** RT-qPCR results from our own collection, consisting of 25 pCR patients and 90 non-pCR patients. The two vertical lines represent the median values of pCR and non-pCR, respectively. **D.** DNAJC12 expression in HR+ and HR- patients in four GEO datasets. **E.** Scatter plots indicating the correlation between DNAJC12 and ESR1 according to RT-qPCR results. **F.** RT-qPCR results of DNAJC12 mRNA levels in the normal breast epithelial cell line MCF 10A and 5 breast cancer cell lines with different molecular subtypes. ER: estrogen receptor; PR: progesterone receptor; HER2: Human epidermal growth factor receptor. **G.** Western blot measuring DNAJC12 protein levels in the normal breast epithelial cell line MCF 10A and 5 breast cancer cell lines with different molecular subtypes. ***, $P < 0.01$.

Comprehensive details are outlined in Table S4. The integrated examination of these datasets, employing Boruta analysis, revealed that DNAJC12 held the highest importance weight among the entire transcriptomic profiles concerning neoadjuvant chemotherapy-related characteristics (Fig. 1A). Additionally, DNAJC12 exhibited significantly higher expression in non-pathological complete response (non-pCR) patients than in pathological complete response (pCR) patients in each of the four datasets ($P < 0.05$) (Fig. 1B).

To confirm the significance of DNAJC12, 115 breast cancer patients undergoing neoadjuvant chemotherapy in our hospital were enrolled, and their clinicopathological characteristics are detailed in Table 1. In accordance with previous findings, the relative expression levels of DNAJC12 in non-pCR patients were markedly elevated compared to those in pCR patients ($P < 0.05$) (Fig. 1C). Subsequently, these 115 patients were categorized into three groups based on the median values of the pCR and non-pCR cohorts. The high DNAJC12-expressing group (constituting 43 % of the total patients) reached a mere 8 % pCR rate, while the low DNAJC12-expressing group (32 %) exhibited a notably higher rate of 38 %. The medium expression group (25 % of the total patients) manifested a pCR rate of 28 %, with no significant deviation from the whole set (24 %).

Moreover, a multivariate logistic regression analysis incorporating five relevant factors based on statistically significant variables from the univariate analysis (Table S5) and their clinical implications was

Table 1
The characteristics of patients.

	pCR (25)	non-pCR (90)	p
Age			> **0.05**
<50	**13**	**56**	
≥50	**12**	**34**	
Tumor size			> **0.05**
T1-T2	**15**	**40**	
T3	**3**	**15**	
T4	**7**	**35**	
Node Status			> **0.05**
Negative	**2**	**9**	
Positive	**23**	**81**	
Clinical Stage			> **0.05**
II	**12**	**25**	
III	**13**	**65**	
ER status			< **0.05***
+	**11**	**68**	
-	**14**	**22**	
PR status			> **0.05**
+	**14**	**62**	
-	**11**	**28**	
HER2 status			< **0.05***
+	**14**	**27**	
-	**11**	**63**	
Ki67 status			> **0.05**
≤20 %	**1**	**14**	
> 20 %	**24**	**76**	
NAC regimens			< **0.05***
PE × 4–6	**13**	**26**	
TEC × 4–6	**12**	**64**	

Note: *$p < 0.05$.

conducted. Remarkably, high expression of DNAJC12 emerged as an independent predictive factor for the response to neoadjuvant chemotherapy ($P < 0.05$, odds ratio [OR] = 0.136, 95 % confidence interval [CI] = 0.035–0.524) (Table 2).

Given the reported regulation of DNAJC12 by hormone receptors, a reanalysis of the association between DNAJC12 expression and hormone receptor (HR) status was performed across each of the four datasets. The HR-positive group exhibited significantly higher expression of DNAJC12 (Fig. 1D). Additionally, a correlation analysis utilizing reverse transcription–quantitative polymerase chain reaction (RT–qPCR) results for ESR1 and DNAJC12 revealed positive correlations between the two (Fig. 1E). Furthermore, an analysis of DNAJC12-associated risk for nonpCR in HR-positive and HR-negative groups separately (Fig. S1) demonstrated a significant elevation of DNAJC12 expression in the nonpCR group compared to the pCR group in HR-positive groups of GEO datasets GSEA25065, GSE20194, and in the validation set from West China Hospital ($P < 0.05$).

3.2. DNAJC12 promotes BC cell proliferation and DOX resistance

To comprehensively investigate the role of DNAJC12 in breast cancer progression and treatment response, we first checked its endogenous expression across distinct molecular subtypes of breast cancer cell lines (Fig. 1F and G). The results revealed that DNAJC12 expression was most pronounced in estrogen receptor (ER)-positive cells and least pronounced in triple-negative cells, consistent with the higher expression observed in hormone receptor-positive (HR+) patients. Subsequently, we modulated DNAJC12 expression in MDA-MB-231 and MCF-7 cells by employing lentivirus, either overexpressing DNAJC12 or short hairpin RNA (shRNA) targeting the DNAJC12 sequence. The efficiency of overexpression and knockdown was validated at both the mRNA and protein levels (Fig. 2A and B).

We proceeded to explore the impact of DNAJC12 on cell proliferation, apoptosis, and drug sensitivity individually. The results from the Cell Counting Kit-8 (CCK-8) and colony formation assays demonstrated that overexpression of DNAJC12 in MDA-MB-231 cells significantly augmented proliferation, a trend similarly observed in the MCF-7 control group when compared with the DNAJC12-treated group (Fig. 2C–E). Flow cytometry results, without any treatment, indicated minimal differences between the negative control (NC) and overexpression (OE) groups of MDA-MB-231, while in MCF-7 cells, there was minimal distinction between the NC and DNAJC12 knockdown groups (SH1) but no discernible difference between the NC and another DNAJC12 knockdown group (SH2) (Fig. 2F and G).

To investigate the influence of DNAJC12 on chemotherapy drugs, we conducted sensitivity assays for doxorubicin (DOX), one of the most common anthracyclines, and docetaxel, one of the most common taxanes, across various molecular types of breast cancer. This included MDA-MB-231 cells overexpressing DNAJC12 and BT-474, SK-BR-3, and MCF-7 cells transfected with DNAJC12 small interfering RNA (siRNA). The interference efficiency is depicted in Fig. 2H and I. The results from the DOX sensitivity assay indicated that DNAJC12 promoted chemoresistance to DOX in these four breast cancer cell lines (Fig. 2J) but exhibited no significant impact on docetaxel (Fig. 2K). The half maximal inhibitory concentration (IC50 value) of DOX underwent notable changes, from 160.8 nM to 31 nM, 66.45 nM–15.57 nM, and 2672 nM–893.1 nM upon DNAJC12 interference in BT474, SKBR3, and MCF-7 cells, respectively. Conversely, in MDA-MB-231 cells overexpressing DNAJC12, the IC50 increased from 16.18 to 82.95 nM.

3.3. DNAJC12 causes DOX resistance in BC by blocking both ferroptosis and apoptosis

To delve deeper into the mechanism underlying DNAJC12's role in breast cancer chemotherapy resistance, we employed RNA sequencing (RNA-seq) to scrutinize transcriptome alterations in MDA-MB-231 cells overexpressing DNAJC12 and negative controls (GEO: accession number GSE191110). Pathway enrichment analysis revealed associations with the SLC-mediated transmembrane transport pathway, lipid biosynthesis, and metabolism-related pathways, particularly linked with ferroptosis, a recently identified cell death pathway involving lipid peroxidation (Fig. 3A). Intriguingly, gene set enrichment analysis (GSEA) demonstrated a positive correlation between DNAJC12 overexpression and ferroptosis pathways, with differential expression of numerous ferroptosis inhibitors (Fig. 3B and Fig. S2A).

Considering previous findings that doxorubicin (DOX) can elevate Fe^{2+} levels and induce reactive oxygen species (ROS) accumulation

Table 2
Multivariate Logistic Regression Analysis of response of NAC.

Variable	Regression Coefficient (B)	The Standard Deviation (SE)	Wald Value	*P*	The *OR* Value	95 %CI
ER	−1.432	0.649	4.866	0.027*	0.239	0.067–0.852
PR	0.145	0.663	0.048	0.827	1.156	0.315–4.242
Ki67	1.473	1.149	1.644	0.2	4.362	0.459–41.471
NAC regimens	−1.342	0.548	5.986	0.014*	0.261	0.089–0.766
DNAJC12			8.599	0.014*		
DNAJC12 (1)	−0.395	0.597	0.438	0.508	0.674	0.209–2.171
DNAJC12 (2)	−1.992	0.687	8.404	0.004*	0.136	0.035–0.524

Note: *$p < 0.05$.

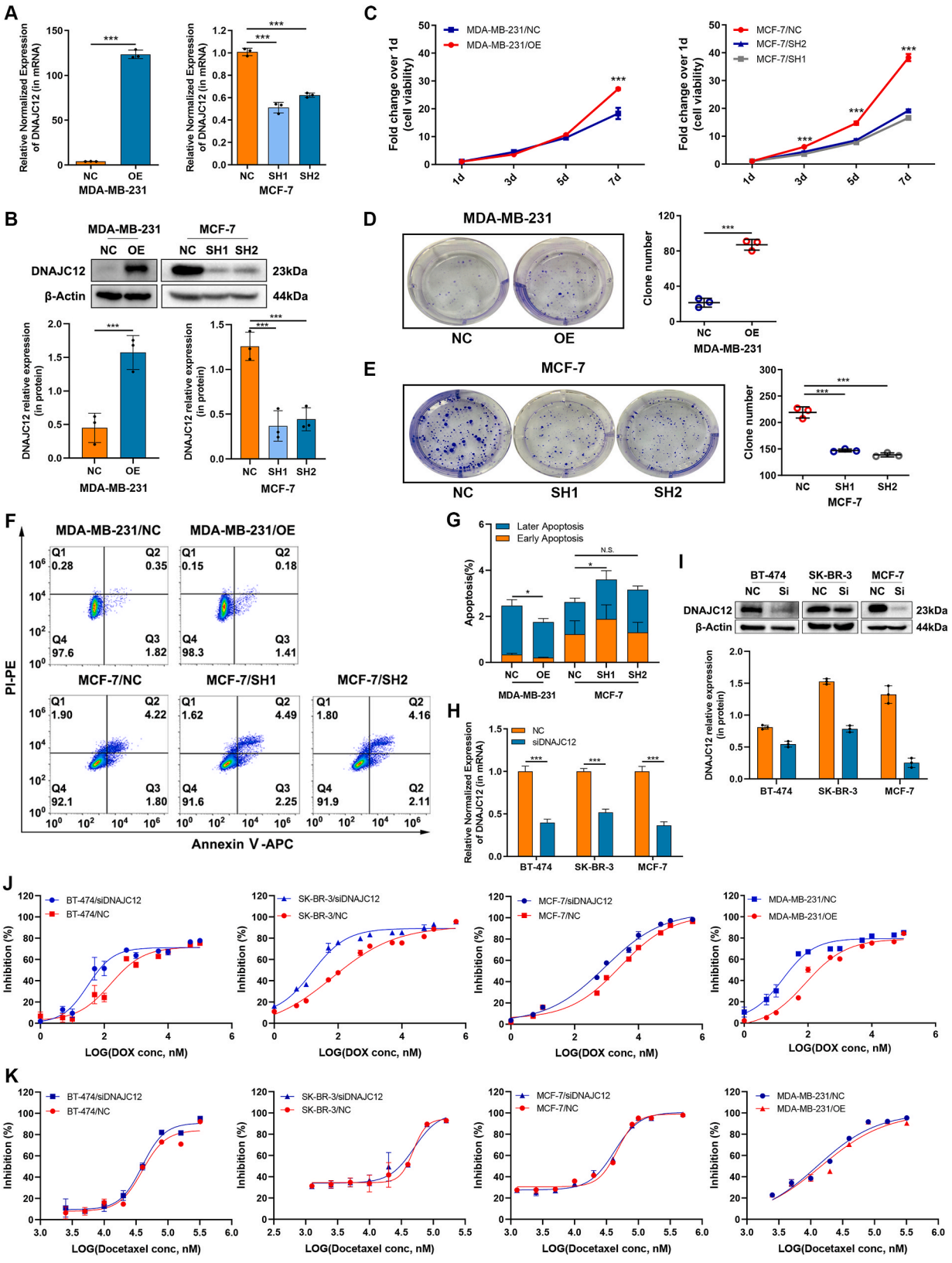

Fig. 2. DNAJC12 promotes cell proliferation and DOX resistance. A. RT-qPCR and **B.** Western blot results showing DNAJC12 levels in MDA-MB-231 cells transfected with DNAJC12v, and MCF-7 cells transfected with shDNAJC12. **C.** Cell growth measured by CCK-8. **D.** Colony formation assay of MDA-MB-231 and **E.** MCF-7, along with the corresponding statistics of colony numbers. **F.** Flow cytometry assay of cell apoptosis without any treatment after 48 h and **G.** the corresponding statistics of apoptosis. **H.** mRNA and **I.** protein levels of DNAJC12 in BT-474, SK-BR-3, and MCF-7 cells interfered with siDNAJC12. **J.** Drug sensitivity assays of doxorubicin and **K.** docetaxel in different breast cancer cells. ***, $P < 0.01$; *, $P < 0.05$; N·S., $P > 0.05$.

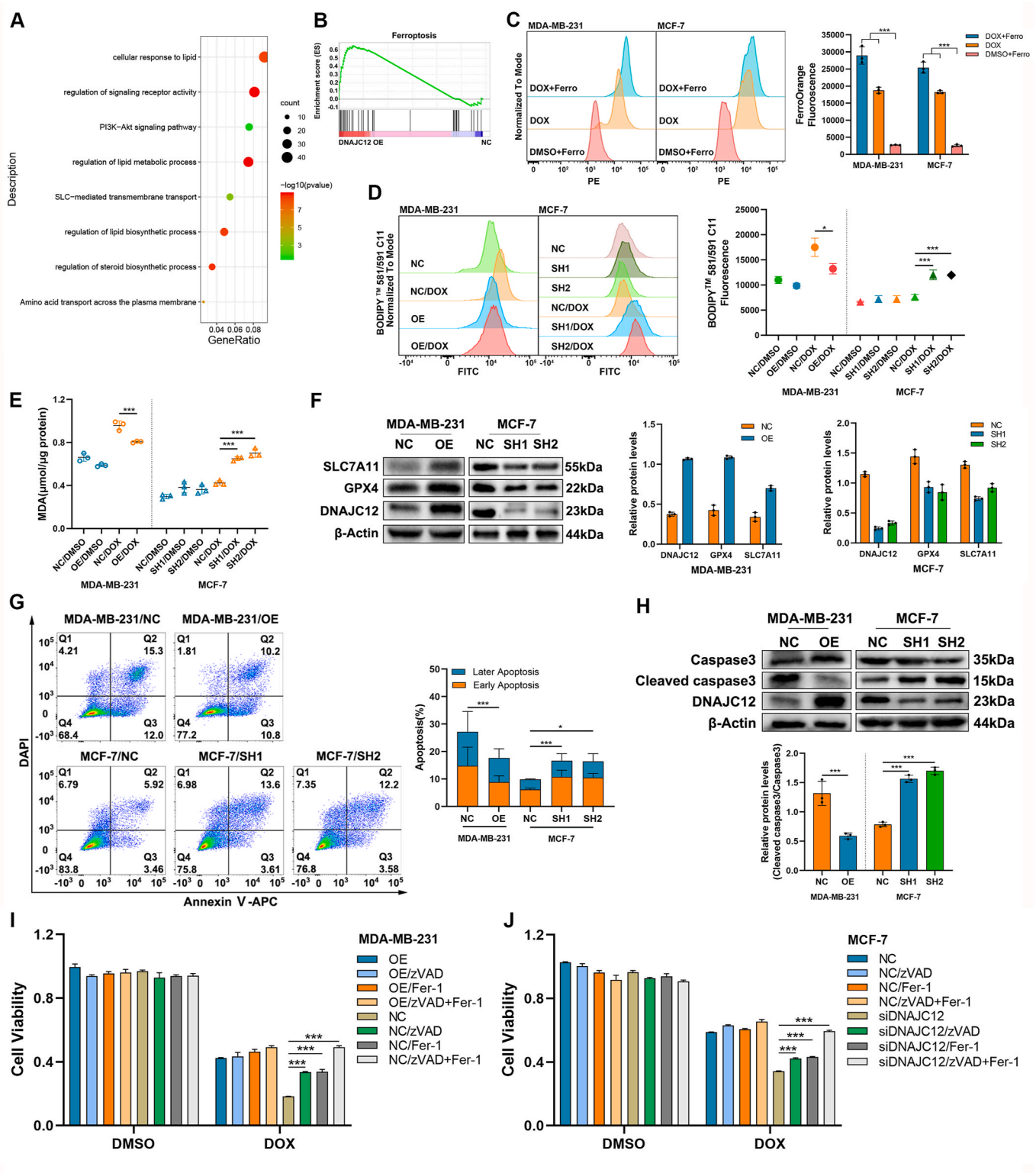

Fig. 3. DNAJC12 causes DOX resistance in BC cells via blocking both ferroptosis and apoptosis. A. Pathway enrichment of RNA-seq in MDA-MB-231 cells overexpressing DNAJC12 compared with the negative control. **B.** GSEA of RNA-seq showed enrichment in the ferroptosis pathway. **C.** Flow cytometry assay stained with a Fe^{2+} fluorescent probe in MDA-MB-231 cells treated with 50 nM DOX and MCF-7 cells treated with 1 μM DOX. **D.** Flow cytometry assay stained with BODIPY 581/591 C11 in MDA-MB-231 cells treated with 50 nM DOX and MCF-7 cells treated with 1 μM DOX to detect lipid peroxidation levels. **E.** Concentrations of MDA were detected in the presence of 50 nM DOX in MDA-MB-231 and 1 μM DOX in MCF-7. **F.** Western blot results of the ferroptosis inhibitor proteins GPX4 and SLC7A11 without any treatment. **G.** Flow cytometry assay and **H.** Western blot results of the apoptosis-related protein cleaved caspase 3 were used to analyze apoptosis in the presence of 50 nM DOX in MDA-MB-231 and 1 μM DOX in MCF-7. **I.** Cell viability measured by CCK-8 after cells were treated with 2 μM Fer, 5 μM zVAD, or a combination of Fer and zVAD in the presence or absence of 50 nM DOX in MDA-MB-231. **J.** Cell viability measured by CCK-8 after cells were treated with 2 μM Fer, 5 μM zVAD, or a combination of Fer and zVAD in the presence or absence of 1 μM DOX in MCF-7. ***, $P < 0.01$; *, $P < 0.05$.

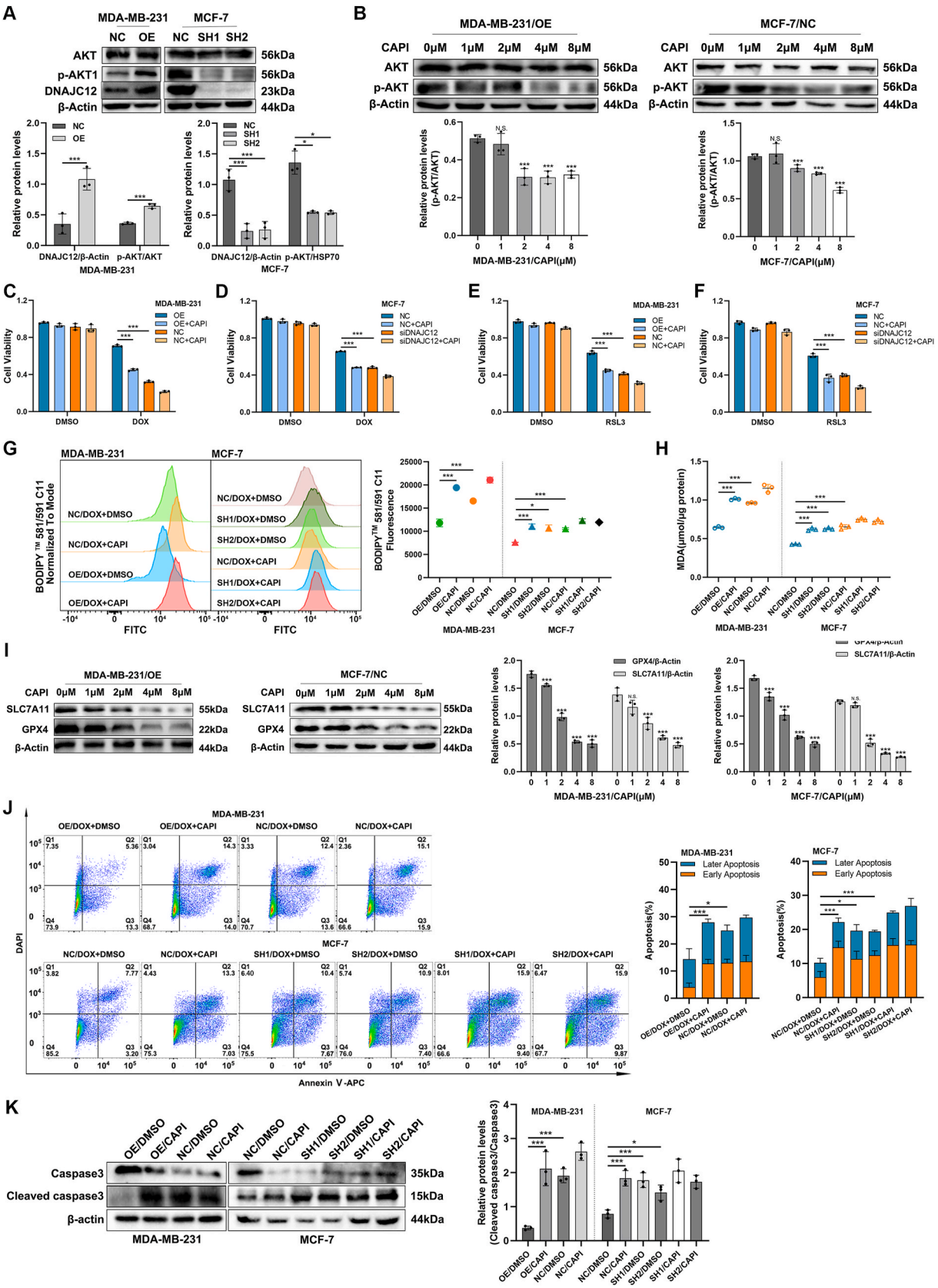

(caption on next page)

Fig. 4. DNAJC12 promotes ferroptosis and apoptosis by upregulating phosphorylation of AKT. A. Western blot measuring the phosphorylation level of AKT. **B.** Western blot measuring the inhibitory effect of AKT inhibitor at different concentrations. **C.** Cell viability measured by CCK-8 after cells were treated with or without 0.1 μM CAPI in the presence or absence of 50 nM DOX in MDA-MB-231. **D.** Cell viability measured by CCK-8 after cells were treated with or without 0.1 μM CAPI in the presence or absence of 1 μM DOX in MCF-7. **E.** Cell viability measured by CCK-8 after cells were treated with or without 0.1 μM CAPI in the presence or absence of 2 μM RSL3 in MDA-MB-231. **F.** Cell viability measured by CCK-8 after cells were treated with or without 0.1 μM CAPI in the presence or absence of 10 μM RSL3 in MCF-7. **G.** BODIPY 581/591 C11 and **H.** MDA concentrations were used to detect lipid peroxidation levels after treatment with or without 0.1 μM CAPI in the presence or absence of 50 nM DOX in MDA-MB-231, and 1 μM DOX in MCF-7. **I.** Western blot results of the ferroptosis inhibitor proteins GPX4 and SLC7A11 after treatment with CAPI at different concentrations. **J.** Flow cytometry assay and **K.** Western blot results of the apoptosis-related protein cleaved caspase 3 were used to analyze apoptosis in cells treated with or without 0.1 μM CAPI in the presence or absence of 50 nM DOX in MDA-MB-231, and 1 μM DOX in MCF-7. ***, $P < 0.01$; *, $P < 0.05$; N·S., $P > 0.05$.

through the Fenton reaction, a crucial process in ferroptosis, we postulated that DNAJC12 might influence DOX cytotoxicity via ferroptosis. Notably, treatment with DOX for 48 h resulted in increased fluorescence intensity of Fe^{2+} in both MDA-MB-231 and MCF-7 cells (Fig. 3C). Given that lipid peroxidation is a hallmark of ferroptosis, we utilized the BODIPY 581/591C11 probe to detect oxidized lipids. Flow cytometry analysis revealed that DNAJC12 knockdown in MCF-7 cells increased lipid peroxidation levels after DOX treatment, while DNAJC12 overexpression in MDA-MB-231 cells decreased lipid peroxidation levels following DOX treatment (Fig. 3D). This observation was corroborated by the detection of malondialdehyde (MDA) levels, the end product of lipid peroxidation, in stable cell lines (Fig. 3E).

To ascertain that the observed changes in lipid reactive oxygen species (ROS) were attributed to ferroptosis, not only apoptosis, we evaluated the response to the ferroptosis inducer RSL3. The results from CCK-8 assays indicated that DNAJC12 overexpression in MDA-MB-231 cells conferred higher cell viability after RSL3 treatment, whereas DNAJC12 knockdown in MCF-7 cells resulted in lower cell viability compared to their respective controls (Fig. S2B). Subsequent analysis using the BODIPY 581/591 C11 probe and MDA levels corroborated these findings (Figs. S2C–E). As observed previously, GPX4 and SLC7A11 were two of the most common ferroptosis inhibitors. We also confirmed that DNAJC12 regulated ferroptosis by regulating GPX4 or SLC7A11 expression. Notably, the protein expression levels of GPX4 and SLC7A11 were significantly elevated in MDA-MB-231 cells overexpressing DNAJC12 and reduced in MCF-7 cells with DNAJC12 knockdown (Fig. 3F).

While apoptosis is recognized as a common mechanism for DOX-induced cell death and GSEA of RNA-seq data revealed a strong association between apoptosis and DNAJC12 (Fig. S2F), we investigated whether DNAJC12 could also influence DOX cytotoxicity through apoptosis. Flow cytometry results indicated that DNAJC12 overexpression in MDA-MB-231 cells led to a lower apoptosis rate under DOX treatment compared to the negative control, whereas DNAJC12 knockdown in MCF-7 cells resulted in a higher apoptosis rate than the negative control (Fig. 3G). This finding was further confirmed by detecting the expression level of cleaved caspase 3, a common apoptotic indicator (Fig. 3H).

Based on these results, we hypothesized that DNAJC12 induces DOX resistance in breast cancer cells by simultaneously inhibiting both ferroptosis and apoptosis. A rescue assay conducted in MDA-MB-231 and MCF-7 cells supported this hypothesis, revealing that ferroptosis inhibitor (Fer-1) and apoptosis inhibitor (zVAD) partly rescued the cytotoxic effect of DOX in both the MDA-MB-231 NC group and MCF-7 siDNAJC12 group, with the combination of the two inhibitors entirely rescuing this effect (Fig. 3I and J). Overall, these findings suggest that DNAJC12 confers DOX resistance in breast cancer cells by blocking apoptosis and ferroptosis simultaneously.

3.4. DNAJC12 inhibits ferroptosis and apoptosis by activating AKT

To elucidate how DNAJC12 regulates apoptosis and ferroptosis induced by doxorubicin (DOX), we conducted a reanalysis of RNA-seq data from MDA-MB-231 cells overexpressing DNAJC12 and its control. This analysis highlighted the PI3K-AKT pathway (Fig. 3A), which is known to suppress apoptosis and ferroptosis through distinct downstream pathways [28,29]. Consequently, we explored whether DNAJC12 inhibits DOX-induced ferroptosis and apoptosis via the activation of AKT. Phosphorylation levels of AKT were assessed in MDA-MB-231 cells overexpressing DNAJC12 and MCF-7 cells with DNAJC12 knockdown. The results demonstrated that DNAJC12 upregulation increased AKT phosphorylation in MDA-MB-231 cells, while DNAJC12 downregulation decreased AKT phosphorylation in MCF-7 cells (Fig. 4A).

Subsequently, we investigated whether DOX resistance induced by DNAJC12 could be reversed by AKT inhibitors, such as capivasertib (CAPI). Preliminary experiments determined an appropriate dose of the AKT inhibitor for subsequent assays (Fig. 4B). A rescue assay revealed that the combined use of CAPI significantly decreased cell viability in the DNAJC12-overexpressing group, approaching the level observed with DOX treatment alone in the negative control group (Fig. 4C). Similarly, in MCF-7 cells, the combined use of CAPI decreased cell viability in the negative control group, approaching the level observed with DOX treatment alone in the DNAJC12 knockdown group (Fig. 4D). These findings indicated that CAPI could reverse DOX resistance induced by DNAJC12.

We then checked whether the inhibition of ferroptosis by DNAJC12 could be reversed by an AKT inhibitor. A CCK-8 assay was used to measure cell viability after RSL3 treatment alone and in combination with CAPI. We found that in MDA-MB-231 cells, CAPI reduced cell viability in the DNAJC12-overexpressing group, approaching that of the negative control group (Fig. 4E). Similarly, in MCF-7 cells, CAPI reduced cell viability in the negative control group, approaching that in the DNAJC12 knockdown group (Fig. 4F). Furthermore, using the BODIPY 581/591 C11 probe to examine lipid peroxidation levels after treatment with DOX alone or combined with CAPI, we observed that the combination use of CAPI with DOX increased lipid peroxidation levels in both the MDA-MB-231 OE group and MCF-7 NC group, approaching those seen with DOX treatment alone in the MDA-MB-231 NC group and MCF-7 SH groups (Fig. 4G). Similarly, consistent trends were observed when evaluating the level of MDA (Fig. 4H). We also used the BODIPY 581/591 C11 probe to examine lipid peroxidation levels after treatment with RSL3 alone or in combination with CAPI. We observed that the combination use of CAPI with RSL3 increased lipid peroxidation levels in both the MDA-MB-231 OE group and MCF-7 NC group, approaching those seen with RSL3 treatment alone in the MDA-MB-231 NC group and MCF-7 SH groups, as well as the level of MDA (Figs. S3A–B). Additionally, Western blot analysis demonstrated that CAPI dose-dependently reduced the protein expression of GPX4 and SLC7A11 in MDA-MB-231 cells overexpressing DNAJC12 and MCF-7 negative control cells (Fig. 4I).

Having established that AKT regulates ferroptosis via DNAJC12, we explored whether AKT also regulates apoptosis in breast cancer cells. Flow cytometry results demonstrated that the use of CAPI in MDA-MB-231 cells overexpressing DNAJC12 increased the apoptosis rate and elevated the expression level of cleaved caspase 3 induced by DOX. Similar effects were observed in MCF-7 cells, where CAPI increased the apoptosis rate and the expression level of cleaved caspase 3 induced by DOX in the negative control group (Fig. 4J and K). In summary, these findings revealed that DNAJC12 inhibits ferroptosis and apoptosis by

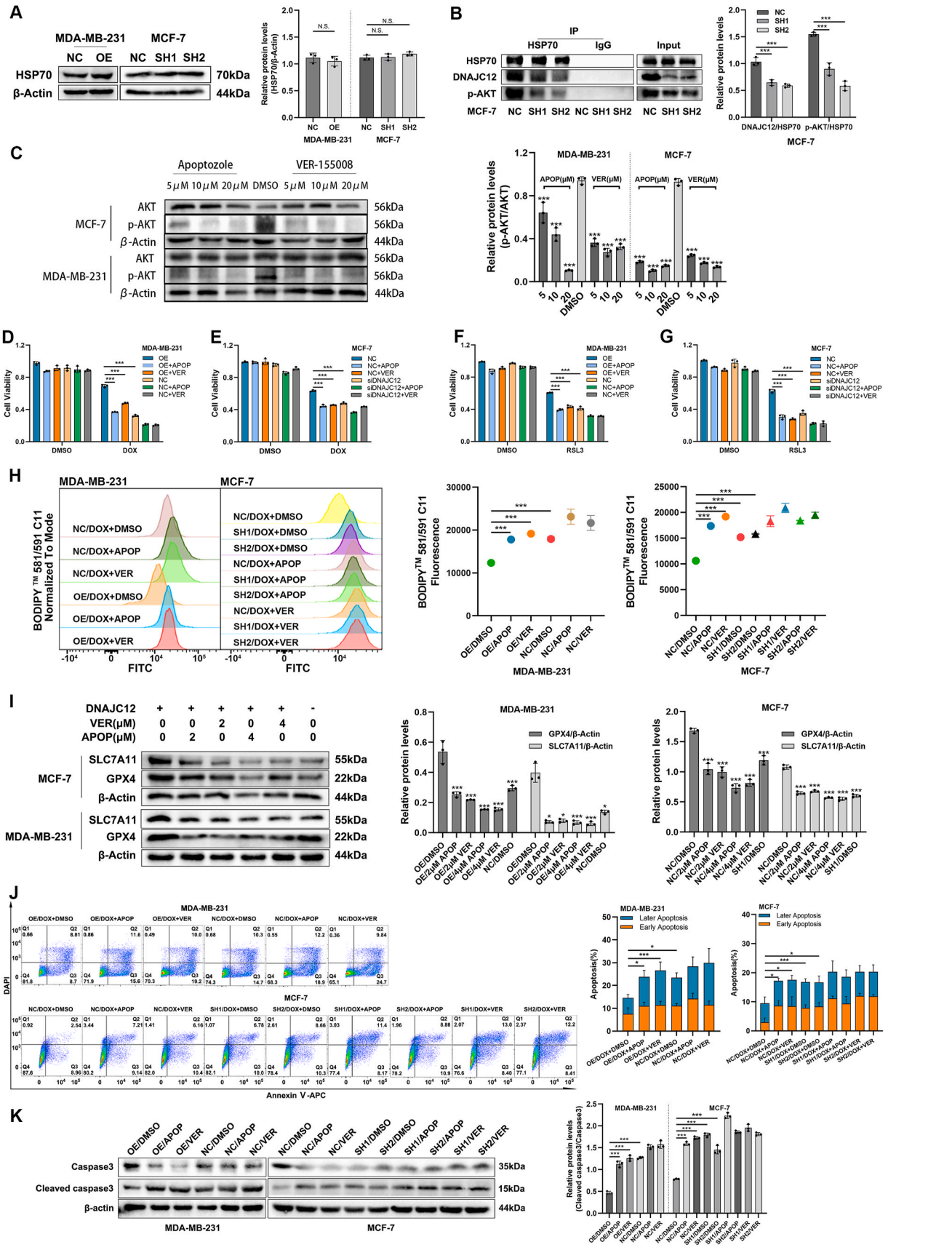

(caption on next page)

Fig. 5. DNAJC12 up-regulates phosphorylation of AKT via activation of HSP70. A. Western blot measuring the phosphorylation level of HSP70. **B.** Co-IP results of MCF-7 using an HSP70 antibody. **C.** Western blot measuring the phosphorylation level of AKT after treatment with HSP70 inhibitors at different concentrations. **D.** Cell viability measured by CCK-8 after cells were treated with or without 2 μM APOP, VER in the presence or absence of 50 nM DOX in MDA-MB-231. **E.** Cell viability measured by CCK-8 after cells were treated with or without 2 μM APOP, VER in the presence or absence of 1 μM DOX in MCF-7. **F.** Cell viability measured by CCK-8 after cells were treated with or without 2 μM APOP, VER in the presence or absence of 2 μM RSL3 in MDA-MB-231. **G.** Cell viability measured by CCK-8 after cells were treated with or without 2 μM APOP, VER in the presence or absence of 10 μM RSL3 in MCF-7. **H.** BODIPY 581/591 C11 was used to detect lipid peroxidation levels after treatment with or without 2 μM APOP, VER in the presence or absence of 50 nM DOX in MDA-MB-231, and 1 μM DOX in MCF-7. **I.** Western blot results of ferroptosis inhibitor proteins GPX4 and SLC7A11 after treatment with 2 μM or 4 μM APOP or VER. **J.** Flow cytometry assay and **K.** Western blot results of cleaved caspase 3 were used to analyze apoptosis in cells treated with or without 2 μM APOP, VER in the presence or absence of 50 nM DOX in MDA-MB-231, and 1 μM DOX in MCF-7. ***, $P < 0.01$; *, $P < 0.05$; N·S., $P > 0.05$.

increasing AKT phosphorylation. Pharmacological inhibition of AKT phosphorylation promotes DOX-induced ferroptosis and apoptosis in breast cancer cells.

3.5. DNAJC12 upregulates the phosphorylation of AKT through activating HSP70

Previously, DNAJC12 has been predominantly recognized as a cochaperone of HSP70, and since HSP70 has been reported to extend the activation of *p*-AKT [30], we posited that DNAJC12 upregulates AKT phosphorylation through HSP70, thereby inducing resistance to doxorubicin (DOX). To investigate the interplay between DNAJC12 and HSP70, we initially examined whether DNAJC12 could influence the expression level of HSP70. Notably, as depicted in Fig. 5A, DNAJC12 did not alter the protein expression level of HSP70. Subsequently, to ascertain whether DNAJC12 physically interacts with HSP70 and influences its activation, a coimmunoprecipitation (co-IP) assay employing an HSP70 antibody was conducted to pull down its binding partners in MCF-7 cells. The co-IP results demonstrated that HSP70 could coprecipitate with DNAJC12 and *p*-AKT simultaneously. Knocking down DNAJC12 in MCF-7 cells resulted in a diminished interaction between HSP70 and *p*-AKT (Fig. 5B). Additionally, two HSP70 inhibitors, Apoptozole and VER-155008, with the former not inhibiting the interaction between HSP70 and ASK1, AIF, JNK, and BAX [31], were used in MDA-MB-231 and MCF-7 wild-type cells in a dose-dependent manner. Both inhibitors downregulated the phosphorylation of AKT in both cell lines (Fig. 5C), suggesting that DNAJC12 upregulates AKT phosphorylation by activating HSP70.

Subsequently, we explored whether DNAJC12-induced DOX resistance is mediated through the upregulation of AKT phosphorylation by activating HSP70. As anticipated, the CCK-8 results revealed that the HSP70 inhibitors Apoptozole and VER-155008 increased the sensitivity of cells to DOX in the DNAJC12-overexpressing group of MDA-MB-231 cells (Fig. 5D). Similar results were observed in the MCF-7 negative control group (Fig. 5E). We further investigated whether HSP70 was involved in DNAJC12-regulated ferroptosis and apoptosis in breast cancer cells separately. First, we examined ferroptosis through an RSL3 drug sensitivity assay. The results demonstrated that the use of apoptozole and VER-155008 reduced cell viability in the DNAJC12-overexpressing group in MDA-MB-231 cells, approaching the levels observed in the negative control group (Fig. 5F). Similarly, in MCF-7 cells, the use of apoptozole and VER-155008 reduced cell viability in the negative control group, approaching that in the DNAJC12 knockdown group (Fig. 5G). Further examination using the BODIPY 581/591 C11 probe to assess lipid peroxidation levels indicated that the coadministration of apoptozole and VER-155008 with DOX increased lipid peroxidation in both the DNAJC12 OE group of MDA-MB-231 cells and the NC group of MCF-7 cells, approaching the levels seen with DOX treatment alone in the MDA-MB-231 NC group and MCF-7 SH groups (Fig. 5H). Similarly, consistent trends were observed when evaluating the level of MDA (Fig. S4A). Additionally, the BODIPY 581/591 C11 probe test and the assessment of malondialdehyde (MDA) levels were conducted after treatment with RSL3 alone or in combination with apoptozole and VER-155008 in MDA-MB-231 and MCF-7 cells. The results showed that apoptozole and VER-155008 could increase the levels of lipid peroxidation and MDA induced by RSL3 in the MDA-MB-231 OE group and MCF-7 NC group (Figs. S4B–C). Previously, we demonstrated that an AKT inhibitor could dose-dependently reduce the protein expression of GPX4 and SLC7A11. To explore whether HSP70 was also involved in this process, MDA-MB-231 OE cells and MCF-7 NC cells were treated with Apoptozole and VER-155008 in a dose-dependent manner, followed by Western blot detection. The results showed that apoptozole and VER-155008 could reduce GPX4 and SLC7A11 protein expression in a dose-dependent manner (Fig. 5I).

For apoptosis, flow cytometry results indicated that the use of apoptozole and VER-155008 in MDA-MB-231 cells overexpressing DNAJC12 increased the apoptosis rate and elevated the expression level of cleaved caspase 3 induced by DOX. Similarly, in MCF-7 cells, apoptozole and VER-155008 increased the apoptosis rate and the expression level of cleaved caspase 3 induced by DOX in the negative control group (Fig. 4J and K). In summary, these findings reveal that DNAJC12 upregulates the phosphorylation of AKT by activating HSP70, leading to the inhibition of ferroptosis and apoptosis induced by DOX.

3.6. AKT inhibitor reverses DNAJC12-induced DOX resistance in vivo

To further substantiate that DNAJC12-induced drug resistance operates through the AKT signaling pathway, subcutaneous tumor mouse models were established. The study employed doxorubicin (DOX) in combination with the AKT inhibitor capivasertib (CAPI) to reverse the DOX resistance induced by DNAJC12. A schematic illustrating intraperitoneal injection is presented in Fig. 6A. After a 15-day treatment period, the average tumor volumes for the eight groups—OE, OE/CAPI, NC, NC/CAPI, OE/DOX, NC/DOX, OE/DOX + CAPI, NC/DOX + CAPI—were recorded as 1461.66, 1083.99, 693.24, 546.65, 399.73, 259.80, 210.51, and 123.49, respectively (Fig. 6B and C). In the growth curve, when treated with DOX alone, the tumor volume in the OE group was twice that of the NC group ($P < 0.05$), indicating that DNAJC12 induced DOX resistance *in vivo*, consistent with previous *in vitro* results. However, when DOX was combined with CAPI in the OE group, the tumor volume was reduced by 5 times compared with DOX alone in the OE group ($P < 0.01$), while exhibiting no significant difference from DOX treatment alone in the NC group ($P > 0.05$). This suggests that the combination of DOX and CAPI in the OE group successfully reversed the DOX resistance caused by DNAJC12. Furthermore, immunohistochemical analysis of tumor samples from the DNAJC12 OE and NC groups revealed an upregulation in the protein expression of *p*-AKT, GPX4, and SLC7A11, consistent with the *in vitro* results (Fig. 6D). These *in vivo* findings further confirmed that DOX resistance is induced by DNAJC12 and that the combination of an AKT inhibitor and DOX can effectively overcome this chemotherapy resistance.

4. Discussion

Among breast cancer patients treated with chemotherapeutic drugs, ER-positive patients tend to be less sensitive to chemotherapeutic drugs than triple-negative and HER2-positive subtypes. In our research, the expression of DNAJC12 was positively correlated with ESR1, consistent with previous studies showing that DNAJC12 mRNA expression is directly associated with the ER status in breast tumors and might be

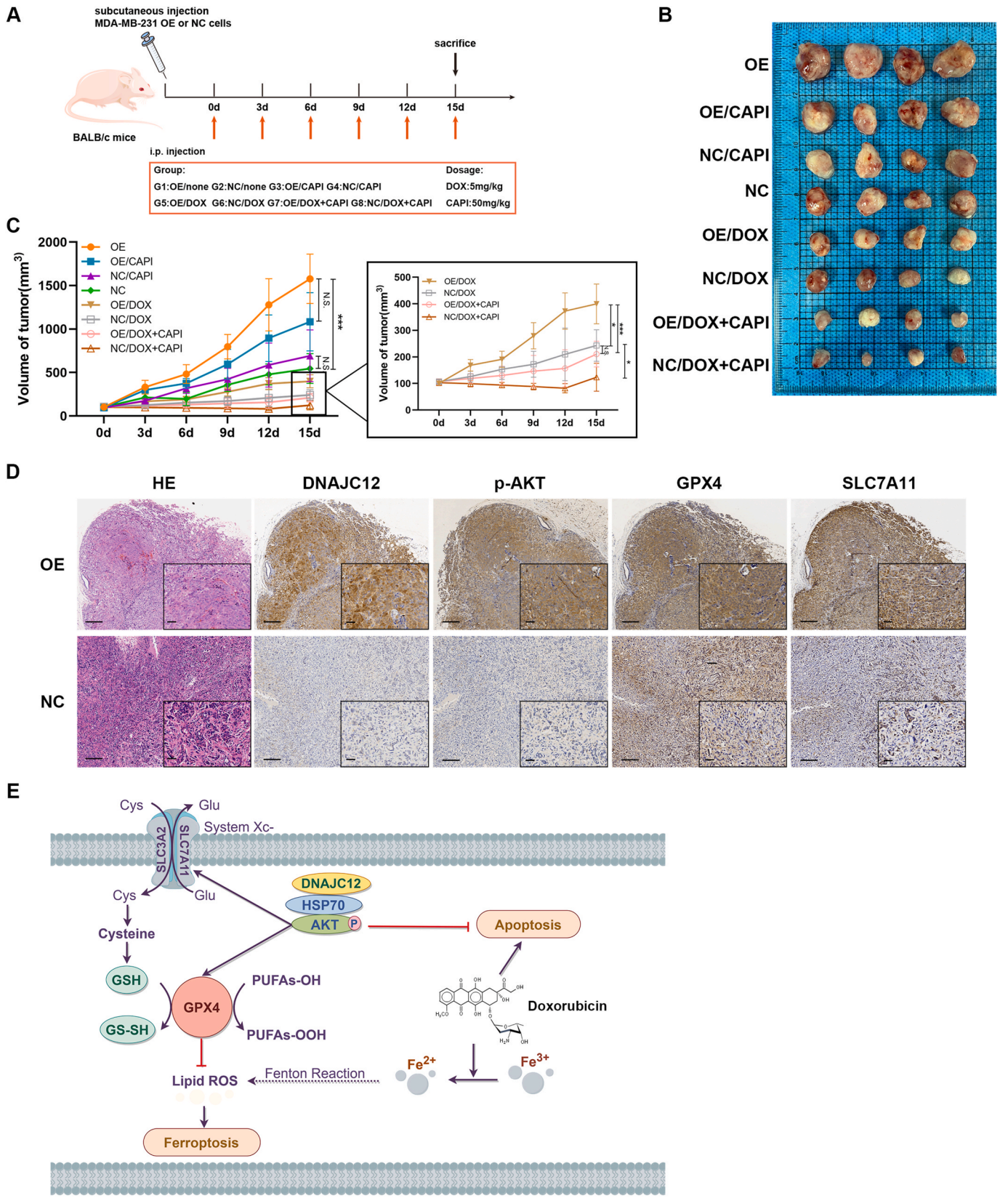

Fig. 6. AKT inhibitor reverses DNAJC12-induced DOX-resistance in vivo. A. Schematic representation of the drug administration schedule for the xenograft tumor model. **B.** Image of resected tumors from mice in different treated groups. **C.** Volume analysis of primary mice tumors in different treated groups. **D.** DNAJC12, *p*-AKT, GPX4, and SLC7A11 expressions were determined by IHC in the tumor sections of MDA-MB-231 OE and NC groups without any treatment. Scale bars: 200 μm. **E.** Model depicting the DNAJC12/HSP70/AKT axis induced doxorubicin resistance via inhibiting ferroptosis and apoptosis.

transcriptionally regulated by estrogen [8,9]. In a previous study of rectal cancer patients, DNAJC12 overexpression acted as a negative predictive factor for the response to neoadjuvant CCRT [15], of which 5-fluorouracil was the key chemotherapeutic agent. In our study, this ER-regulated gene was strongly linked with the chemotherapy response of breast cancer patients both in GEO datasets and our RT–qPCR results.

To elucidate the underlying mechanism, we performed RNA-seq, and GSEA results showed that the apoptosis and ferroptosis pathways were positively correlated with significant overexpression of DNAJC12. The AKT pathway was also enriched. Apoptosis is the most important mechanism of cell death induced by DOX. Likewise, the relationship between the AKT signaling pathway and apoptosis has been reported in many studies, including apoptosis induced by DOX [12].

In addition to the induction of apoptosis, it was also reported that DOX may cause severe toxicities, such as cardiomyopathy and heart failure, which could be avoided by reducing ferroptosis. Notably, this study confirmed the induction of ferroptosis by DOX. Our research found that DNAJC12 is associated with ferroptosis in cells and could elevate the expression of two important ferroptosis inhibition proteins, GPX4 and SLC7A11, thus reducing lipid peroxidation to ultimately inhibit RSL3-induced ferroptosis. Intriguingly, as we mentioned above, DNAJC12 has been reported to be associated with a variety of neurological diseases. A growing number of studies are looking at the link between ferroptosis and several neurodegenerative diseases [17]. Coupling between dopamine synthesis and packaging may be closely regulated by DNAJC12 [32]. In addition, dopamine was reported to increase the stability of GPX4, thus inhibiting ferroptosis [33]. In our research, the overexpression of DNAJC12-induced DOX resistance was partially rescued by apoptosis or ferroptosis inhibitors but could be entirely reversed by a combination of inhibitors of apoptosis and ferroptosis. However, there are few reports on AKT and ferroptosis. Hyperactivation of the PI3K-AKT-mTOR pathway regulates SREBP1/SCD1-mediated lipogenesis, leading to the inhibition of oxidative stress and ferroptosis [29]. FG-4592 inhibited ferroptosis through Akt/GSK-3β-mediated Nrf2 activation at the early stage of folic acid-induced kidney injury [34]. Blocking AKT activity induced ACSL4 expression in sh-SIRT3 cells, which led to ferroptosis [35]. In addition, the Akt/Nrf2/Gpx4 pathway was reported to be a protective pathway of exogenous Mel treatment in HIBD [36].

Hsp70s are ubiquitous molecular chaperones that play important roles in folding and remodeling processes of a variety of cellular proteins and protect cells from damage in response to various stress stimuli [37]. The main function of DNAJC12 is to stimulate the ATPase activity of Hsp70 through its J-domain [38]. However, because its domain organization shares only the J-domain with a paradigm member of the HSP40 family, it can bind with Hsp70 and perform activities not necessarily related to general protein folding [37]. In LNCaP cells, immunoprecipitation experiments showed the interaction of the endogenous DNAJC12 and Hsc70 proteins [39]. In our research, co-IP also showed the combination of HSP70 and DNAJC12 as well as AKT. Different expression levels of DNAJC12 could influence the binding of DNAJC12 and phosphorylated AKT. The peptide-binding domain of Hsp70 interacts with the AKT protein on its dephosphorylated turn motif, prolongs the lifetime of active AKT and sustains its function [30]. Several reports have shown that the Hsp70 level and its ATPase function could regulate the level and activity of AKT in different ways [40–44]. HSP70-induced AKT activation was involved in many drug-induced apoptosis processes in previous studies [45,46]. Heat shock 70-kDa protein 5 (HSPA5) increased the expression and activity of glutathione peroxidase 4 (GPX4) and thus inhibited ferroptosis [47,48]. A similar phenomenon was observed in our study.

In conclusion, our study is the first to demonstrate that DOX kills cancer cells via ferroptosis and reveals that DNAJC12 can cause breast cancer chemotherapy resistance by repressing DOX-induced ferroptosis and apoptosis. The DNAJC12/HSP70/AKT regulatory axis could induce DOX resistance by inhibiting both ferroptosis and apoptosis (Fig. 6E). Meanwhile, our results further supported the efficacy of AKT inhibitors or HSP70 inhibitors in reversing this process. These findings may provide a new perspective on DOX resistance in ER-positive breast cancer or other molecular subtypes with high expression of DNAJC12. Regarding limitations, whether HSP70 can also regulate the phosphorylation of AKT by affecting the expression or activity of upstream kinases or the downstream pathway of *p*-AKT remains to be further studied.

CRediT authorship contribution statement

Mengjia Shen: Conceptualization, Investigation, Writing – original draft. **Shiyu Cao:** Methodology, Validation. **Xinyi Long:** Methodology, Visualization. **Lin Xiao:** Data curation, Methodology. **Libo Yang:** Data curation, Formal analysis. **Peichuan Zhang:** Software, Visualization. **Li Li:** Methodology. **Fei Chen:** Methodology. **Ting Lei:** Formal analysis, Visualization. **Hongwei Gao:** Supervision. **Feng Ye:** Project administration, Writing – review & editing. **Hong Bu:** Funding acquisition, Project administration, Supervision.

Declaration of competing interest

The authors declare no potential conflicts of interest.

Data availability

Data will be made available on request.

Acknowledgments

The work was supported by the 1.3.5 project for disciplines of excellence, West China Hospital, Sichuan University (ZYGD18012, ZYJC21035, ZYGX2022YGRH015). The authors would like to thank Huifang Li and Yan Wang (Core Facility of West China Hospital) for their help with the flow cytometry measurements.

Appendix A. Supplementary data

Supplementary data to this article can be found online at https://doi.org/10.1016/j.redox.2024.103035.

References

[1] H. Sung, J. Ferlay, R.L. Siegel, M. Laversanne, I. Soerjomataram, A. Jemal, et al., Global cancer statistics 2020: GLOBOCAN Estimates of incidence and mortality worldwide for 36 cancers in 185 countries, CA A Cancer J. Clin. 71 (3) (2021) 209–249.
[2] V. Romeo, G. Accardo, T. Perillo, L. Basso, N. Garbino, E. Nicolai, et al., Assessment and prediction of response to neoadjuvant chemotherapy in breast cancer: a comparison of imaging modalities and future perspectives, Cancers 13 (14) (2021).
[3] W.D. Foulkes, I.E. Smith, J.S. Reis-Filho, Triple-negative breast cancer, N. Engl. J. Med. 363 (20) (2010) 1938–1948.
[4] J. Lee, Y. Hahn, J.H. Yun, K. Mita, J.H. Chung, Characterization of JDP genes, an evolutionarily conserved J domain-only protein family, from human and moths, Biochim. Biophys. Acta 1491 (1–3) (2000) 355–363.
[5] W.L. Kelley, Molecular chaperones: how J domains turn on Hsp70s, Curr. Biol. 9 (8) (1999) R305–R308.
[6] A.L. Fink, Chaperone-mediated protein folding, Physiol. Rev. 79 (2) (1999) 425–449.
[7] S.E. Wardell, V. Boonyaratanakornkit, J.S. Adelman, A. Aronheim, D.P. Edwards, Jun dimerization protein 2 functions as a progesterone receptor N-terminal domain coactivator, Mol. Cell Biol. 22 (15) (2002) 5451–5466.
[8] S.A. De Bessa, S. Salaorni, D.F.C. Patrão, M.M. Neto, M.M. Brentani, M.A. Nagai, JDP1 (DNAJC12/Hsp40) expression in breast cancer and its association with estrogen receptor status, Int. J. Mol. Med. 17 (2) (2006) 363–367.
[9] M. Lin, Y.-N. Wang, Y. Ye, Z. Xiong, F. Guo, H. Chen, DNAJC12 as a mediator between ESR1 and ERBB4 in breast carcinoma cells, Front. Oncol. 11 (2021) 582277.
[10] D. Euhus, D. Bu, X.-J. Xie, V. Sarode, R. Ashfaq, K. Hunt, et al., Tamoxifen downregulates ets oncogene family members ETV4 and ETV5 in benign breast tissue: implications for durable risk reduction, Cancer Prev. Res. 4 (11) (2011) 1852–1862.
[11] C.K. Cajigas-Du Ross, S.R. Martinez, L. Woods-Burnham, A.M. Durán, S. Roy, A. Basu, et al., RNA sequencing reveals upregulation of a transcriptomic program

associated with stemness in metastatic prostate cancer cells selected for taxane resistance, Oncotarget 9 (54) (2018) 30363–30384.
[12] H. Sun, H.-Y. Zou, X.-Y. Cai, H.-F. Zhou, X.-Q. Li, W.-J. Xie, et al., Network analyses of the differential expression of heat shock proteins in glioma, DNA Cell Biol. 39 (7) (2020) 1228–1242.
[13] Y. Uno, M. Kanda, T. Miwa, S. Umeda, H. Tanaka, C. Tanaka, et al., Increased expression of DNAJC12 is associated with aggressive phenotype of gastric cancer, Ann. Surg Oncol. 26 (3) (2019) 836–844.
[14] Y. Li, M. Li, F. Jin, J. Liu, M. Chen, J. Yin, DNAJC12 promotes lung cancer growth by regulating the activation of β-catenin, Int. J. Mol. Med. 47 (6) (2021).
[15] H.-L. He, Y.-E. Lee, H.-P. Chen, C.-H. Hsing, I.W. Chang, Y.-L. Shiue, et al., Overexpression of DNAJC12 predicts poor response to neoadjuvant concurrent chemoradiotherapy in patients with rectal cancer, Exp. Mol. Pathol. 98 (3) (2015) 338–345.
[16] S.J. Dixon, K.M. Lemberg, M.R. Lamprecht, R. Skouta, E.M. Zaitsev, C.E. Gleason, et al., Ferroptosis: an iron-dependent form of nonapoptotic cell death, Cell 149 (5) (2012) 1060–1072.
[17] H.-F. Yan, T. Zou, Q.-Z. Tuo, S. Xu, H. Li, A.A. Belaidi, et al., Ferroptosis: mechanisms and links with diseases, Signal Transduct. Targeted Ther. 6 (1) (2021) 49.
[18] S. Bannai, E. Kitamura, Transport interaction of L-cystine and L-glutamate in human diploid fibroblasts in culture, J. Biol. Chem. 255 (6) (1980) 2372–2376.
[19] S. Doll, M. Conrad, Iron and ferroptosis: a still ill-defined liaison, IUBMB Life 69 (6) (2017) 423–434.
[20] A. Scirè, L. Cianfruglia, C. Minnelli, D. Bartolini, P. Torquato, G. Principato, et al., Glutathione compartmentalization and its role in glutathionylation and other regulatory processes of cellular pathways, Biofactors 45 (2) (2019) 152–168.
[21] D. Giustarini, F. Galvagni, A. Tesei, A. Farolfi, M. Zanoni, S. Pignatta, et al., Glutathione, glutathione disulfide, and S-glutathionylated proteins in cell cultures, Free Radic. Biol. Med. 89 (2015) 972–981.
[22] V.S. Viswanathan, M.J. Ryan, H.D. Dhruv, S. Gill, O.M. Eichhoff, B. Seashore-Ludlow, et al., Dependency of a therapy-resistant state of cancer cells on a lipid peroxidase pathway, Nature 547 (7664) (2017) 453–457.
[23] Z. Wang, Y. Ding, X. Wang, S. Lu, C. Wang, C. He, et al., Pseudolaric acid B triggers ferroptosis in glioma cells via activation of Nox 4 and inhibition of xCT, Cancer Lett. 428 (2018) 21–33.
[24] A. Varela-López, M. Battino, M.D. Navarro-Hortal, F. Giampieri, T.Y. Forbes-Hernández, J.M. Romero-Márquez, et al., An update on the mechanisms related to cell death and toxicity of doxorubicin and the protective role of nutrients, Food Chem. Toxicol. 134 (2019) 110834.
[25] X. Fang, H. Wang, D. Han, E. Xie, X. Yang, J. Wei, et al., Ferroptosis as a target for protection against cardiomyopathy, Proc. Natl. Acad. Sci. U. S. A. 116 (7) (2019) 2672–2680.
[26] T. Tadokoro, M. Ikeda, T. Ide, H. Deguchi, S. Ikeda, K. Okabe, et al., Mitochondria-dependent ferroptosis plays a pivotal role in doxorubicin cardiotoxicity, JCI Insight 5 (9) (2020).
[27] D. Jardine, M. Antolovich, P.D. Prenzler, K. Robards, Liquid chromatography-mass spectrometry (LC-MS) investigation of the thiobarbituric acid reactive substances (TBARS) reaction, J. Agric. Food Chem. 50 (6) (2002) 1720–1724.
[28] Z. Cheng, S. Yu, W. He, J. Li, T. Xu, J. Xue, et al., Selenite induces cell cycle arrest and apoptosis reactive oxygen species-dependent inhibition of the AKT/mTOR pathway in thyroid cancer, Front. Oncol. 11 (2021) 668424.
[29] J. Yi, J. Zhu, J. Wu, C.B. Thompson, X. Jiang, Oncogenic activation of PI3K-AKT-mTOR signaling suppresses ferroptosis via SREBP-mediated lipogenesis, Proc. Natl. Acad. Sci. U. S. A. 117 (49) (2020) 31189–31197.
[30] T. Gao, A.C. Newton, The turn motif is a phosphorylation switch that regulates the binding of Hsp70 to protein kinase C, J. Biol. Chem. 277 (35) (2002) 31585–31592.
[31] S.-K. Ko, J. Kim, D.C. Na, S. Park, S.-H. Park, J.Y. Hyun, et al., A small molecule inhibitor of ATPase activity of HSP70 induces apoptosis and has antitumor activities, Chem. Biol. 22 (3) (2015) 391–403.
[32] L. Straniero, I. Guella, R. Cilia, L. Parkkinen, V. Rimoldi, A. Young, et al., DNAJC12 and dopa-responsive nonprogressive parkinsonism, Ann. Neurol. 82 (4) (2017) 640–646.
[33] Z. Zhang, J.R. Christin, C. Wang, K. Ge, M.H. Oktay, W. Guo, Mammary-stem-cell-based somatic mouse models reveal breast cancer drivers causing cell fate dysregulation, Cell Rep. 16 (12) (2016) 3146–3156.
[34] X. Li, Y. Zou, J. Xing, Y.-Y. Fu, K.-Y. Wang, P.-Z. Wan, et al., Pretreatment with roxadustat (FG-4592) attenuates folic acid-induced kidney injury through antiferroptosis via akt/GSK-3/nrf2 pathway, Oxid. Med. Cell. Longev. 2020 (2020) 6286984.
[35] L. Liu, Y. Li, D. Cao, S. Qiu, Y. Li, C. Jiang, et al., SIRT3 inhibits gallbladder cancer by induction of AKT-dependent ferroptosis and blockade of epithelial-mesenchymal transition, Cancer Lett. (2021) 510.
[36] Z. Gou, X. Su, X. Hu, Y. Zhou, L. Huang, Y. Fan, et al., Melatonin improves hypoxic-ischemic brain damage through the Akt/Nrf2/Gpx4 signaling pathway, Brain Res. Bull. 163 (2020) 40–48.
[37] R. Rosenzweig, N.B. Nillegoda, M.P. Mayer, B. Bukau, The Hsp70 chaperone network, Nat. Rev. Mol. Cell Biol. 20 (11) (2019) 665–680.
[38] W.L. Kelley, The J-domain family and the recruitment of chaperone power, Trends Biochem. Sci. 23 (6) (1998) 222–227.
[39] J. Choi, S. Djebbar, A. Fournier, C. Labrie, The co-chaperone DNAJC12 binds to Hsc70 and is upregulated by endoplasmic reticulum stress, Cell Stress Chaperones 19 (3) (2014) 439–446.
[40] J. Koren, U.K. Jinwal, Y. Jin, J. O'Leary, J.R. Jones, A.G. Johnson, et al., Facilitating Akt clearance via manipulation of Hsp70 activity and levels, J. Biol. Chem. 285 (4) (2010) 2498–2505.
[41] M. Kayama, T. Nakazawa, A. Thanos, Y. Morizane, Y. Murakami, S. Theodoropoulou, et al., Heat shock protein 70 (HSP70) is critical for the photoreceptor stress response after retinal detachment via modulating anti-apoptotic Akt kinase, Am. J. Pathol. 178 (3) (2011) 1080–1091.
[42] H. Kukreti, K. Amuthavalli, A. Harikumar, S. Sathiyamoorthy, P.Z. Feng, R. Anantharaj, et al., Muscle-specific microRNA1 (miR 1) targets heat shock protein 70 (HSP70) during dexamethasone-mediated atrophy, J. Biol. Chem. 288 (9) (2013) 6663–6678.
[43] G. Hu, J. Tang, B. Zhang, Y. Lin, J.-I. Hanai, J. Galloway, et al., A novel endothelial-specific heat shock protein HspA12B is required in both zebrafish development and endothelial functions in vitro, J. Cell Sci. 119 (Pt 19) (2006) 4117–4126.
[44] J. Martin, J. Masri, A. Bernath, R.N. Nishimura, J. Gera, Hsp70 associates with Rictor and is required for mTORC2 formation and activity, Biochem. Biophys. Res. Commun. 372 (4) (2008) 578–583.
[45] L. Liu, Y. Huang, X. Feng, J. Chen, Y. Duan, Overexpressed Hsp70 alleviated formaldehyde-induced apoptosis partly via PI3K/Akt signaling pathway in human bronchial epithelial cells, Environ. Toxicol. 34 (4) (2019) 495–504.
[46] X. He, Z. Lin, J. Ning, N. Li, X. Cui, B. Zhao, et al., Promoting TTC4 and HSP70 interaction and translocation of annexin A7 to lysosome inhibits apoptosis in vascular endothelial cells, Faseb. J. 34 (9) (2020) 12932–12945.
[47] Y. Chen, Y. Mi, X. Zhang, Q. Ma, Y. Song, L. Zhang, et al., Dihydroartemisinin-induced unfolded protein response feedback attenuates ferroptosis via PERK/ATF4/HSPA5 pathway in glioma cells, J. Exp. Clin. Cancer Res. 38 (1) (2019) 402.
[48] S. Zhu, Q. Zhang, X. Sun, H.J. Zeh, M.T. Lotze, R. Kang, et al., HSPA5 regulates ferroptotic cell death in cancer cells, Cancer Res. 77 (8) (2017) 2064–2077.